Applied Chemistry Today

Semnan University

Research Article

Green and Environmentally Sustainable Fabrication of CuFe₂O₄/CuO-rGO@EosinY as a Photocatalyst for the Synthesis of Xanthene Derivatives

Effat Samiee Paghaleh, **Eskandar Kolvari**[*]

Department of Chemistry, Semnan University, P.O. Box, 35131-19111 Semnan, Iran

PAPER INFO	ABSTRACT

One of the biggest challenges to the expansion of photochemical processes has been the creation of effective visible-light photocatalysts for organic synthesis. Heterogeneous photocatalysts present a favorable procedure to realize green and eco-friendly organic reactions. We fabricated the heterogenous catalyst CuFe₂O₄/CuO-rGO@EosinY (EY) by immobilizing eosin on the substrate CuFe₂O₄/CuO-rGO. The eosin substrate was made by heating basil seed hydrogel (BSH) that had copper and iron added to it. The prepared heterogeneous catalyst as a photocatalyst was applied in a green one-pot multi-component protocol for the production of biologically important xanthene derivatives via condensation of aromatic aldehydes and dimedone under the condition of visible light irradiation. The synthesized photocatalyst was characterized using various techniques, such as FT-IR, XRD, and TGA. The significant advantages of the present methodology include remarkable yield, cost-effectiveness, easy work-up, broad substrate scope, and significant reusability. The prepared catalyst was used four times without a significant decrease in reaction efficiency.

---

[*] **.Corresponding author:** Associate Professor of Organic Chemistry, Department of Chemistry, Semnan University, Semnan, Iran. *E-mail address: Kolvari@semnan.ac.ir*

1. Introduction

The field of photocatalytic organic synthesis has garnered significant attention from researchers due to its notable selectivity, the use of mild reaction conditions, and its environmentally benign and energy-efficient properties [1]. UV light only makes up around 4% of the total solar energy, whereas visible light makes up about 50%. Chemists have changed the synthesis approach by concentrating on the inclusion of visible light in the last few years as a result of the growing interest in the applications of green principles in organic synthesis [2–5]. However, the majority of organic molecules are unable to absorb visible wavelengths. Hence, the development of photocatalysts capable of harnessing visible light is an imperative area of research from a pragmatic perspective. Visible-light induced extensive research has been conducted on reactions with photoredox catalysts. Additionally, these reactions are good for the environment because they use light-emitting diodes (LEDs) [6], which are energy-efficient light sources, to shine visible light on them and only use small amounts of catalysts.

Homogeneous photocatalysts have been extensively studied and have been found to have a significant role in photoredox catalysis [6–8]. Due to their unique active sites homogeneous photocatalysts have shown great promise in a wide range of organic transformations. However, these materials also encounter practical challenges, including the toxicity of metals, elevated expenses, potential product contamination, and limitations in terms of reusability. These factors impede their widespread implementation in chemical industries on a large scale. Currently, there is a growing interest in the design and utilization of heterogeneous catalysts as a means to address and overcome these challenges [9]. There are three main methods for creating effective heterogeneous visible light photocatalysts: (1) Extensive band gap semiconductors can change their optical responses from the UV to the visible range by doping them with metal or non-metal components [10, 11]. (2) One popular technique for creating visible light photocatalysts is the coupling of semiconductors with various band gaps [12, 13]. (3) Organic dyes can make semiconductors sensitive to photocatalytic activity when exposed to visible light [14, 15]. In the aforementioned visible light-catalyzed reaction, the use of affordable organic dyes as catalysts has recently increased [16]. In visible light-induced photoredox catalysis, the redox properties of the excited state of the dye molecules are usually used. Consequently, they are also capable of acting as a thermal-redox agent without the use of light [17]. EY is an organic dye that has been successfully utilized in the design of numerous photoreduction catalysts. An anionic dye in the fluorescein family, EY is acidic. Organophotocatalyst EY is a readily available, affordable, and well-known product. It has been demonstrated that dye sensitization increases the range of visible light and encourages photoconversion [14].

Carbon-functionalized materials like graphene oxide and reduced graphene oxide (rGO) have recently emerged as viable options to produce innovative composite materials due to their high specific area, high thermal stability, and biocompatibility [18, 19]. RGO has been demonstrated to have stronger catalytic activity when combined with semiconductors than several other materials [18, 20]. It is very good at conducting electrons, which means that it speeds up the process of getting electrons out of semiconductors and lowers the chance of electron-hole pair recombination [21]. In contrast to covalent functionalization, graphene can be noncovalently functionalized by molecular

interactions such as л-л stacking, electrostatic interaction, and hydrogen bonding without substantially changing the system. This preserves the extended л conjugation on the graphene surface. Dye sensitization of semiconductors is a successful method for extending the spectrum of excitation energy of semiconductors into the visible region as a technique for effective visible light harvesting [22, 23]. The dye molecules that have been adsorbed on the semiconductor gather energy and transport electrons to the semiconductor's conduction band. EY is often available as a disodium salt or in its neutral form. Hydrogen bonds, stacking, and halogen bonding are used to attach the EY molecule to reduced graphene oxide [24].

Multi-component reactions (MCRs) are a crucial and fundamental area within the domain of organic transformations [26-28]. The authors have garnered significant acclaim for their successful amalgamation of crucial heterocyclic chemicals and medicinal molecules [29, 30]. Xanthenes possess considerable significance as heterocyclic compounds due to their extensive utilization in the realms of biology and industry. The literature has recognized these compounds for their anti-inflammatory activities [31] and their ability to demonstrate antibacterial actions [20]. Because of their wide range of pharmacological activity and also their industrial and synthetic applications, several methods have been reported for the synthesis of xanthene, which include trapping of benzynes by phenols [29, 30], cyclodehydration [31] between 2-hydroxyaromatic aldehydes and 2-tetralone [32], and intramolecular phenyl carbonyl coupling reactions of benzaldehyde and acetophenones [33]. One of the most common and uncomplicated procedures for synthesizing xanthenes is the condensation reaction of aldehydes with cyclic 1,3-dicarbonyl compounds. In the

literature, different catalysts for making xanthene derivatives have been described. These include sulfamic acid/MCM-41, cellulose sulfamic acid, and SnO_2/TiO_2 [25].

In this study, EY was immobilized on reduced graphene oxide for the first time without using covalent bonds. The carbonaceous material used came from activated basil seeds (Ocimum basilicum L.). These seeds were chosen due to their advantageous characteristics, such as being ecologically friendly, readily available, cost-effective, and renewable biomass. As a substrate, $CuFe_2O_4/CuO$-rGO was used, and EY was used as a photosensitizer. This was done so that EY could be immobilized without covalent bonds. This photocatalyst, a cost-effective, safe, and readily available option, can be easily recovered. This photocatalyst was used to make multi-component reactions (MCRs) of xanthene derivatives. It worked very well in mild conditions and in a very short amount of time. The catalyst employed in the study was confirmed using analytical techniques such as XRD, FTIR, SEM, EDX, and TGA. The significance of our research lies in its capacity to solve the challenges usually associated with the catalysts presently employed in the synthesis of these compounds. This approach for the synthesis of xanthene derivatives presented in this work provides several significant advantages.

2. Experimental

2.1. Preparation of CuFe₂O₄/CuO‑rGO substrate

We created the $CuFe_2O_4/CuO$-rGO substrate in three steps: (a) we precipitated the metal ions inside the hydrogel; (b) we bonded metal ions to the basil seed hydrogel network to create a 3D network; and (c) we heated the basil seed hydrogel to create the $CuFe_2O_4/CuO$-rGO. In the first stage, basil seed (1 g) was soaked in 100 ml of deionized water for 1 hour and then separated with filter paper. In the next step, it was impregnated with $CuCl_2.2H_2O$ (0.75 g,

4.39 mmol), $FeCl_3.6H_2O$ (0.42 g, 1.55 mmol), and $FeCl_2.4H_2O$ (0.28 g, 1.4 mmol) and stirred for 1 hour at room temperature. After sufficiently chelating, the basil seed hydrogel was collected and rinsed with deionized water until pH neutral. For the second stage, metal ion precipitation, the produced basil seed hydrogel was combined with NaOH (1 M). The metal-precipitated basil seed hydrogels were rinsed with deionized water after 30 minutes of precipitation. The basil seed hydrogels' metal precipitation was introduced to a combustion boat in the third stage, where it was then calcined at 750 °C for 30 min in a vacuum furnace. The sample was then gathered and kept dry while being stored at room temperature [34].

2.2. Preparation of CuFe₂O₄/CuO-rGO@EY catalyst

To prepare the $CuFe_2O_4$/CuO-rGO@EY catalyst, $CuFe_2O_4$/CuO-rGO (0.06 g) was mixed with powder EY (7 mg), and water (2 ml) was added to it and put in ultrasonic for 30 minutes. In the next step, stir for 48 hours. In the end, the mixture was centrifuged and dried in a desiccator for 2 hours.
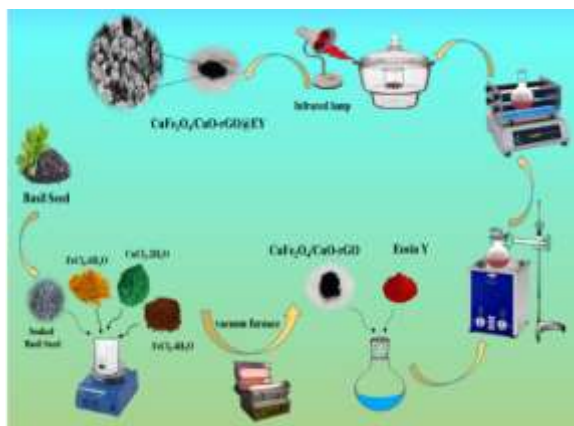
Fig.1. Schematic representation of preparation steps for $CuFe_2O_4$/CuO-rGO@EY [34]

2.3. General Synthesis Route for Xanthene Derivatives

A mixture of aromatic aldehyde (1 mmol), dimedone (1 mmol), and $CuFe_2O_4$/CuO-rGO@EY catalyst (3 mg) in deionized water (3 ml) was added to a round bottom flask. The mixture was irradiated with a red

light-emitting diode (LED) under open-air conditions at 60 °C. After reaction completion (controlled by TLC), the reaction mixture was diluted using toluene (3 mL), the magnetic catalyst was separated using a magnet, and the product was recrystallized.

3. Results and discussion

3. 1. Sample characterization

The structural (e.g. FTIR, XRD), morphological (e.g., SEM), thermal analyses (e.g., TGA) and elemental analysis (e.g., EDX), characterizations were applied for a full investigation of properties of $CuFe_2O_4$/CuO-rGO@ EY.

3.1.1. FTIR analysis

The results of the FTIR analysis, which was carried out to clarify the changes in functional groups before and after the adsorption of dye, are displayed in Fig. 2. The FTIR spectrum's peak position didn't change when the adsorbent adsorption changed, which showed that the same types of functional groups were on the adsorbent surface. The broad band at 3700–3200 cm^{-1} corresponded to the stretching vibration of hydroxyl groups (O–H). The main cause of the broad peak at 1042 cm^{-1} was the structure's alcoholic, phenolic, and carboxylic groups vibrating in a C-O direction. The chemical composition of basil seeds and their functional group were verified. The C-H vibrations, the C-O band, and the C-O-C stretching vibrations of glycosidic linkage of polysaccharides are all related to several peaks that occurred at 1090, 1151, and 1240 cm^{-1}. The uronic acid residues in the basil seed are seen in the bands at 1460 and 1656 cm^{-1}, which are connected to the symmetric and asymmetric stretching vibrations of the COO bond. The C=O symmetric and asymmetric stretching vibrations of carboxylate groups were attributed to two peaks at 1542 and 1745 cm^{-1}, respectively. Two peaks, associated with CH_2 bending vibrations and CH stretching vibrations, appeared at 2931 and 3013

cm^{-1}. It should be noticed that after the basil seed is carbonized, the intensity of all these peaks is noticeably lowered, indicating a successful synthesis of reduced graphene oxide. For the S-scheme of $CuFe_2O_4/CuO$-rGO heterostructure, the chemical structure and the functional group were confirmed by the FT-IR spectrum. It is indicated by the disappearance of absorbance peaks of the O-H group (3162 cm^{-1}). peaks at 1780 and 1448 cm^{-1} for the C=O and C=C groups, respectively. $CuFe_2O_4/CuO$-rGO exhibits octahedral Cu^{2+} (Cu-O mode) stretching vibration with a peak at about 490 cm^{-1}, and tetrahedral Fe^{3+} (Fe-O mode) stretching vibration with a peak at about 643 cm^{-1}[35]. The characteristic peaks of EY at 3400 and 1717 cm^{-1} correspond to the OH of the alcohol group and the C=O stretching vibrations of the lactone tautomer. [40]. C-Br stretching vibration shows peaks at 567 cm^{-1} and 420 cm^{-1} [36]. The peak at 720, 1036 cm^{-1}, and 1445 is attributed to the C-Ar, C-O-C, and C=C vibrations, respectively. It is crucial to understand that EY contains aromatic rings, oxygen groups, and a C-Br bond, all of which support hydrogen bonding [37], halogen bonding [38] , and л-л interaction [39]. The FTIR spectrum also supported the viewpoint. The peak of the aromatic group shifted, maybe owing to the existence of halogen bonding (π-Br) and π-π interaction between carbon active and EY. The paired O-C-O asymmetric stretch of the carboxyl group is responsible for the combined absorption peak at 1632 cm^{-1} that EY displayed. This indicated a significant interaction existed between EY and carbon activity. There may be an ester-like bond between the carboxyl group of EY and the hydroxyl on the surface of reduced graphene oxide.
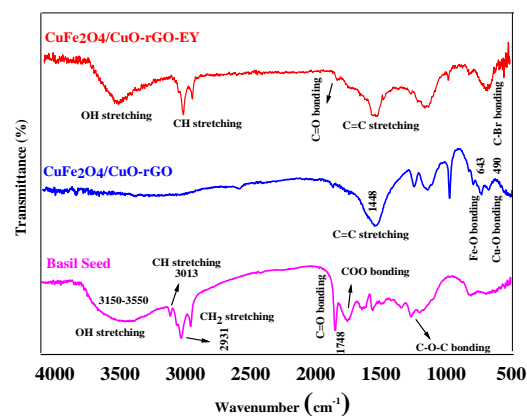

Fig.2. FT-IR spectra samples of $CuFe_2O_4/CuO$-rGO@EY

3.1.2. XRD analysis

An X-ray diffraction (XRD) pattern was used to find out if $CuFe_2O_4/CuO$-rGO@EY was crystalline (Fig. 3). The XRD patterns of the prepared S-scheme $CuFe_2O_4/CuO$-rGO display peaks at $2\theta = 48.87°$, $53.03°$, and $68.20°$ that are ascribed to CuO, and peaks at $2\theta = 30.18°$, $35.65°$, $37.49°$, $62.45°$, and $75.19°$ confirm the presence of $CuFe_2O_4$. The S-scheme $CuFe_2O_4/CuO$-rGO heterostructure's XRD patterns match well with the structure of $CuFe_2O_4$ (JCPDS card No. 00-025-0283) and the structure of CuO (JCPDS card No. 01-080-1916). This means that the nanoparticles were made successfully. Two peaks at $2\theta = 23°$ and $41°$, corresponding to the (002) and (100) planes, confirm the presence of reduced graphene oxide. The central peaks in the $CuFe_2O_4/CuO$-rGO@EY composite have decreased, and their intensity has been reduced in $CuFe_2O_4/CuO$-rGO@EY. This proved that the increase in EY dye in nature is due to the decrease in crystallinity, which results from the reduction in hydrogen linkages between substrate layers [40]. The intermolecular hydrogen bond and л-л are the only interactions possible between the carbon substrate matrix and activated groups in EY dye. These findings are in agreement with previously reported results [41].
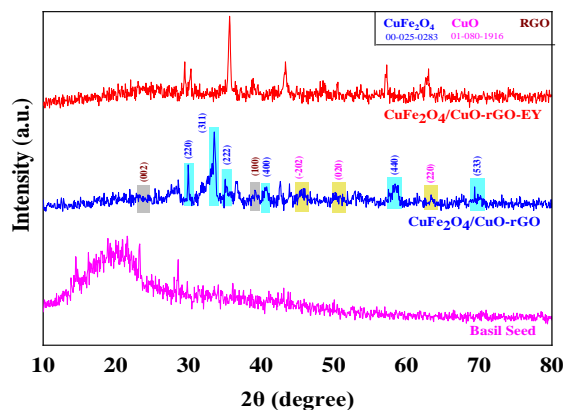
Fig.3. XRD patterns of samples of CuFe$_2$O$_4$/CuO-rGO@EY

3.1.3. TGA analysis

Thermogravimetric analysis (TGA) was conducted to examine the thermochemical behavior of the CuFe$_2$O$_4$/CuO-rGO@EY across a temperature range of 25 to 800 °C. In Figure 4, the TGA curves of CuFe$_2$O$_4$/CuO-rGO@EY before and after EY adsorption are shown. The TGA curve reveals weight loss in the initial stages, which is attributed to the removal of surface-bound OH groups or intercalated water molecules. Between 250 and 500 °C and 500 and 700 °C, the basil seed undergoes two distinct weight loss events, indicating the complete degradation and breakdown of the carbon structure. A minor weight loss is observed between 400 and 700 °C, indicating the thermal stability of the carbonized basil seed. Additionally, a negligible weight loss is observed between 700 and 800 °C, confirming the elimination of residual functional groups. The CuFe$_2$O$_4$/CuO-rGO heterostructure exhibits remarkable thermal stability throughout the TGA analysis, highlighting its suitability for high-temperature applications. The EY component was destroyed at about 200–380 °C. After adsorption of EY onto a substrate, a notable weight loss occurred, about 9 wt% more than CuFe$_2$O$_4$/CuO-rGO.
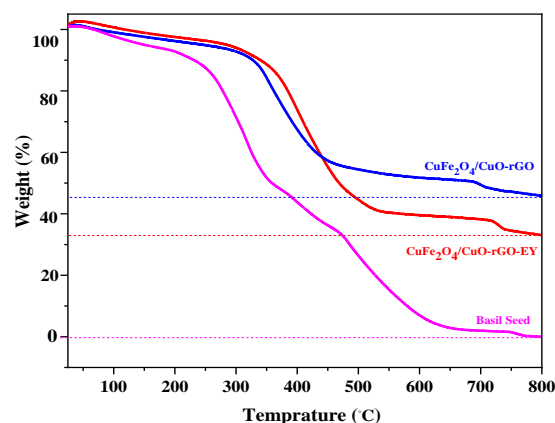

Fig.4. TGA curve of as-prepared samples of CuFe$_2$O$_4$/CuO-rGO@EY

3.1.4. Morphology and elemental analysis

The morphology of the CuFe$_2$O$_4$/CuO-rGO@EY was studied using field emission scanning electron microscopy (FESEM). As displayed in Fig 5(a-c), EY molecules were observed as a sponge on a substrate. Elemental energy-dispersive X-ray spectroscopy (EDS) mapping of the CuFe$_2$O$_4$/CuO-rGO@EY demonstrated the presence and homogeneous distribution of Br, Fe, Cu, C, and O, which are the expected components Fig 5(d, e). Trace amounts of Na, S, N, and P were also detected, likely associated with composition of the basil seed.
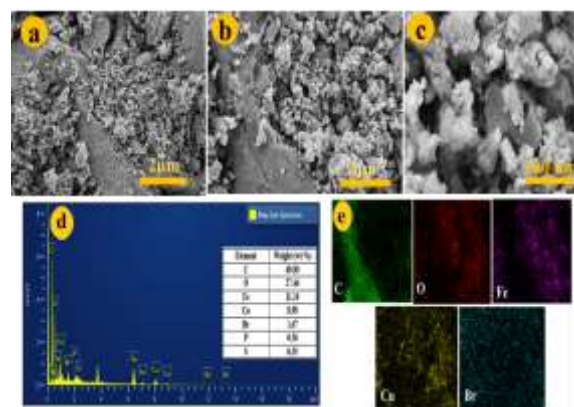

Fig. 5. FESEM images at different magnifications (a-c) and EDX spectra and element mapping images(d,e) of CuFe$_2$O$_4$/CuO-rGO@EY

3.2. The photocatalytic activity of CuFe$_2$O$_4$/CuO-rGO@EY

CuFe$_2$O$_4$/CuO-rGO@EY was used as a photocatalyst in a reaction with benzaldehyde (0.25

mmol) and dimedone (0.5 mmol) while it was exposed to LED light to look into how well it worked (Scheme 1). In a test tube, the reaction mixture was magnetically stirred. To find the best conditions for the condensation reaction, many factors were optimized, such as the irradiation source, the amount of photocatalyst, the type of solvents, and the temperature.
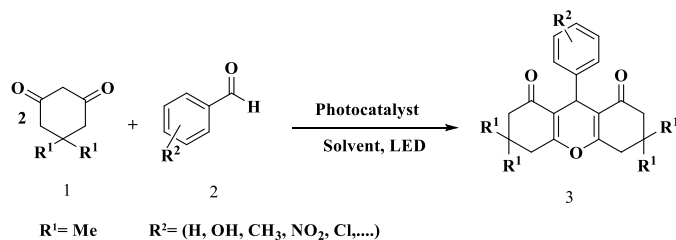
Scheme 1. Synthesis of xanthenes by $CuFe_2O_4$/CuO-rGO@EY

Under red LED light irradiation, favorable results were seen at a temperature of 60 °C in the presence of 3 mg of catalyst in a water solvent (Table 1). The new catalyst was also tested to see if it could be used to make other xanthene derivatives using different aromatic aldehydes (Table 3).

3.3. Studying the effect of the light source

The reaction was exposed to various light irradiations because the irradiation source is one of the key variables impacting the efficacy of photocatalytic reactions (Table 2). Based on the results obtained different yields would be produced under the same conditions if the reaction were conducted in the dark or with some LED lights of different colors. Red LED light irradiation yielded the highest efficiency.
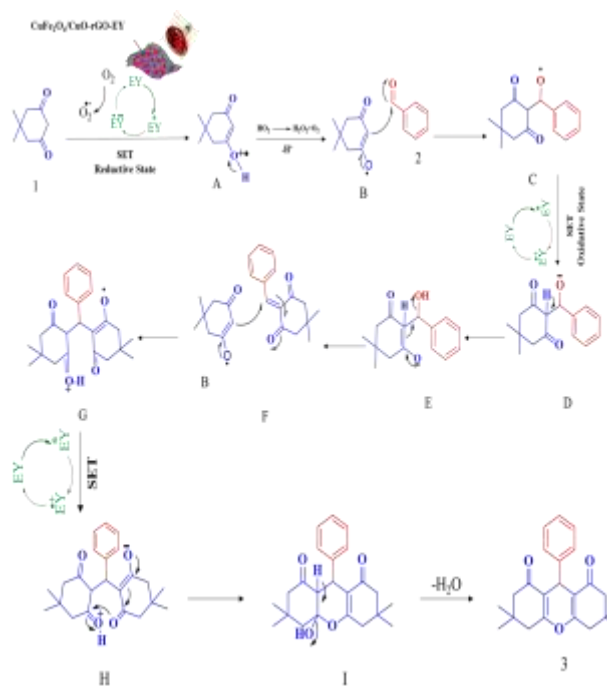
Table 1. Optimization of synthesis of 3,3,6,6-tetramethyl-9-phenyl-3,4,5,6,7,9-hexahydro-1H-xanthene-1,8(2H)-dione condition

Entry	Amount of catalyst (mg)	Solvent	Temperature (°C)	Time (min)	Yield (%)
1	4	H_2O	60	15	98
2	2	H_2O	60	15	80
3	1	H_2O	60	15	50
4	3	H_2O	R.T.	15	20
5	3	H_2O	40	15	50
6	3	Solvent-Free	60	15	NR
7	3	EtOH	60	15	10
8	3	Toluene	60	15	Trace
9	3	CH_3CN	60	15	5
10	**3**	**H_2O**	**60**	**15**	**100**

Table 2. Optimization of the irradiation source in condensation reaction[a]

Entry	Light source	Time (min)	Yield (%)
1	Dark	15	55
2	Blue	15	90
3	Green	15	85
4	**Red**	**15**	**100**

[a] Reaction conditions: benzaldehyde (0.25 mmol), dimedone (0.5 mmol), CuFe$_2$O$_4$/CuO-rGO@EY (3 mg), 60 °C, open atmosphere

Table 3. Synthesis of xanthenes derivatives catalyzed by CuFe$_2$O$_4$/CuO-rGO@EY [a]

Entry	R_2	Time (min)	Yield (%)
1	H	15	100
2	4-CH$_3$	60	90
3	4-Cl	60	100
4	2,4-dichloro	60	99
5	4-O$_2$N	20	100
6	3-O$_2$N	15	100
7	4-HO	45	100
8	4-MeO	60	99
9	3-EtO-4-HO	60	98
10	4-Me$_2$N	60	80
11	1,4-diphenyl	10	100

[a] Reaction conditions: benzaldehyde (0.25 mmol), dimedone (0.5mmol), CuFe$_2$O$_4$/CuO-rGO@EY (3 mg), H_2O (3ml), 60 °C open atmosphere, red LED (3 W, *850* nm)

The production of xanthene was examined using several aqueous and organic solvents. The results indicated that the highest reaction efficiency was achieved when water was used as the solvent. This can be due to the radical reaction of xanthene synthesis that occurs in the presence of light. In the presence of water, the photocatalyst generates holes that lead to the formation of H^+ and $OH^\cdot$ ions as a result of electron excitation. In addition, it has the ability to generate oxygen and facilitate oxidation-reduction reactions, resulting in the production of $O_2/O_2^{\cdot-}$. However, when performed in organic solvents like ethanol, the presence of OH radicals is diminished, leading to a decrease in the reaction's efficiency. The drop in catalyst quantity resulted in a reduction of active sites on the surface of CuFe$_2$O$_4$/CuO-rGO@EY, leading to a decrease in the yield of product production. When the amount of CuFe$_2$O$_4$/CuO-rGO@EY was increased, more light-excited carriers and active sites were made. This improved the photocatalytic performance. As the catalyst concentration continued to increase, the dispersion of light hindered its penetration into the mixture, resulting in a decrease in the product yield. The reaction was examined at various temperatures, namely ambient temperature, 40 degrees, and 60 degrees. As the temperature rises, the abundance of radicals also increases, resulting in an escalation of the reaction rate.

3.4. Reaction mechanism

Scheme 2 shows the likely mechanism for the synthesis of the targeted molecule based on the literature review [42-44]. When exposed to visible light, EY initially changed into the excited state

EY*. This EY* then underwent reductive quenching by 1,3-dicarbonyl (1) to produce the radical cation (A) and form an EY radical anion. To complete the cycle and produce a superoxide radical anion ($O_2^{\bullet-}$), aerobic oxygen oxidized the EY radical anion to its ground state. The radical (B) was produced when ($O_2^{\bullet-}$) deprotonated the resultant radical cation (A). Aldehyde (2) and this radical (B) are now reacting simultaneously to form (C). Single electron transfer (SET) transforms EY into compound (C) to (D), which can function as a michael acceptor by interconverting to dicarbonyl enone (E). Dimedon (B) interacts with chemical F via the SET reaction to produce the radical cation (G). EY then travels through SET to change (G) into (H). Finally, (I) experiences a straightforward reaction by dehydration, producing the Xanthene (3).

rGO@EY provides several advantages, which include exceptional stability, an easy synthesis process, simple catalyst recovery, and recyclability of the catalyst. The described catalysts do, however, offer certain benefits [45-49].

S Scheme 2. A possible mechanism of the synthesis of *xanthene* in the presence of CuFe$_2$O$_4$/CuO-rGO@EY catalyst.

3.5. Comparison of CuFe$_2$O$_4$/CuO-rGO@EY catalyst with other works

A comparative survey of the catalytic efficiency of CuFe$_2$O$_4$/CuO-rGO@EY with previously reported catalysts is depicted in Table 4. CuFe$_2$O$_4$/CuO-

Table 4. Comparison of Catalytic Efficiency of $CuFe_2O_4/CuO$ rGO@EY

Entry	Catalyst	Solvent/Condition	Time (h: min)	Yield (%)	Ref.
1	Fe^{3+}-montmorillonite	EtOH/100 °C	06:00	94	[50]
2	$ZnO-CH_3COCl$	CH3CN/reflux	05:00	86	[51]
3	SO_4^{2-}/ZrO_2	EtOH/70 °C	08:00	86	[52]
4	$Fe_3O_4@SiO_2$-imid-PMAn	EtOH/reflux	01:30	94	[53]
5	$CuFe_2O_4/CuO$-rGO@EY	H_2O/60 °C	00:15	100	This work

3.6. Reusability

One of the important criteria for assessing the effectiveness of catalysts is reusability. When a catalyst can be easily recovered and utilized again, it becomes very important to the industry. For this reason, after the first run was finished, toluene was added, and the catalyst was separated from the reaction mixture using a magnet and dried in an oven at 60 °C before being reused in the same reaction for five additional runs (Fig. 6) to study the stability and reusability of $CuFe_2O_4/CuO$-rGO@EY. It was discovered that the extraction efficiency of $CuFe_2O_4/CuO$-rGO@EY could be recycled five times without suffering significantly. The outcomes demonstrated the $CuFe_2O_4/CuO$-rGO@EY photocatalyst's viability for repeated use
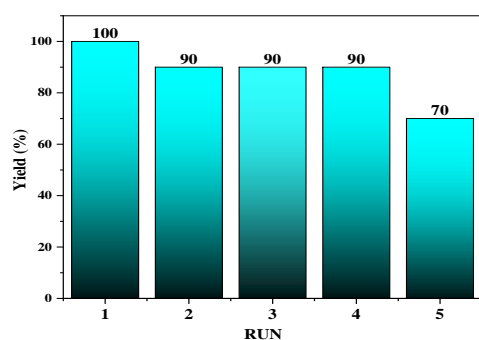
Fig.6. Recycling experiment in the synthesis of xanthene in the presence of $CuFe_2O_4/CuO$-rGO@EY

4. Conclusion

Using the photocatalyst $CuFe_2O_4/CuO$-rGO@EY made it easier to change different aldehydes into xanthenes by using dimedone. The outcomes were quite satisfactory. The selection of solvent, temperature, number, and color of LED lamps for the photocatalyst had a significant impact on the reaction. The optimal condition was determined to be the inclusion of 3 mg of catalyst in a water solvent with a temperature of 60 °C and red LED lighting. The photocatalyst has demonstrated the capacity to be reused and employed in five distinct instances. There was no significant decline in the production output of the product. X-ray diffraction (XRD), Fourier-transform infrared spectroscopy (FTIR), thermogravimetric analysis (TGA), scanning electron microscopy (SEM) with elemental mapping, and a leaching test were employed to verify the accuracy of the photocatalyst. The main benefits of the proposed method are its convenient accessibility and the use of air as the sole eco-friendly oxidizing agent. This strategy functions as a potent and pragmatic alternate pathway for achieving the intended objective. It holds significant value in the domains of organic synthesis, natural product chemistry, and medicinal chemistry.

Conflicts of Interest

The authors declare that they have no known competing financial interests or personal relationships that could have appeared to influence the work reported in this paper.

References

[1] Chen, W., Gu, D., Zhou, T., & Peng, X. (2023). Visible-light-induced sulfoxidation using chitosan-supported organic dyes photocatalyst. *Dyes and Pigments*, *210*, 111042.

[2] Cambie, D., Bottecchia, C., Straathof, N. J., Hessel, V., & Noel, T. (2016). Applications of continuous-flow photochemistry in organic synthesis, material science, and water treatment. *Chemical Reviews, 116*(17), 10276-10341.

[3] Cao, M.-Y., Ren, X., & Lu, Z. (2015). Olefin difunctionalizations via visible light photocatalysis. *Tetrahedron Letter, 56*(24), 3732-3742.

[4] Ghosh, S., Saikh, F., Das, J., & Pramanik, A. K. (2013). Hantzsch 1,4-dihydropyridine synthesis in aqueous ethanol by visible light. *Tetrahedron Letter, 54*(1), 58-62.

[5] König, B. (2017). Photocatalysis in organic synthesis–past, present, and future. *European Journal of Organic Chemistry, 2017*(15), 1979-1981.

[6] Tomoko, Y. (2022). Visible-light-induced Organocatalytic Peruoroalkylation of Electron rich Olefins. *Journal of Synthetic Organic Chemistry, Japan*, *112***,***8610.*

[7] Sharma, S., & Sharma, A. (2019). Recent advances in photocatalytic manipulations of Rose Bengal in organic synthesis. *Organic & Biomolecular Chemistry*, *17*(18), 4384-4405.

[8] Prier, C. K., Rankic, D. A., & MacMillan, D. W. (2013). Visible light photoredox catalysis with transition metal complexes: applications in organic synthesis. *Chemical reviews*, *113*(7), 5322-5363

[9] Srivastava, V., & Singh, P. P. (2017). Eosin Y catalysed photoredox synthesis: a review. *RSC advances*, *7*(50), 31377-31392

[10] Gisbertz, S., & Pieber, B. (2020). Heterogeneous photocatalysis in organic synthesis. *ChemPhotoChem*, *4*(7), 456-475.

[11] Asahi, R., Morikawa, T., Ohwaki, T., Aoki, K., & Taga, Y. (2001). Visible-light photocatalysis in nitrogen-doped titanium oxides. *science, 293*(5528), 269-271.

[12] Hwang, D. W., Kim, H. G., Jang, J. S., Bae, S. W., Ji, S. M., & Lee, J. S. (2004).Photocatalytic decomposition of water–methanol solution over metal-doped layered perovskites under visible light irradiation. *Catalysis Today, 93*, 845-850.

[13] Li, Y., Chen, G., Zhou, C., & Sun, J. (2009). A simple template-free synthesis of nanoporous $ZnS–In_2S_3–Ag_2S$ solid solutions for highly efficient photocatalytic H_2 evolution under visible light. *Chemical Communications,* (15), 2020-2022.

[14] Li, Q., Jin, Z., Peng, Z., Li, Y., Li, S., & Lu, G. (2007). High-efficient photocatalytic hydrogen evolution on eosinY-sensitized Ti−MCM41 zeolite under visible-light irradiation. *Journal of Physical Chemistry C, 111*(23), 8237-8241.

[15] Youngblood, W. J., Lee, S.-H. A., Maeda, K., & Mallouk, T. E. (2009). Visible light water splitting using dye-sensitized oxide

semiconductors. *Accounts of Chemical Research, 42*(12), 1966-1973.

[16] Li, S., Yang, X., Wang, Y., Zhou, H., Zhang, B., Huang, G., Li, Y. (2018). Visible Light-Induced Aerobic Oxidative− H Arylation of Glycine Derivatives. *Advanced Synthesis and Catalysis, 360*(22), 4452-4456.

[17] Kalaitzakis, D., Kouridaki, A., Noutsias, D., Montagnon, T., & Vassilikogiannakis, G. (2015). Methylene Blue as a Photosensitizer and Redox Agent: Synthesis of 5-Hydroxy-1H-pyrrol-2 (5H)-ones from Furans. *Angewandte Chemie International Edition, 54*(21), 6283-6287.

[18] Julkapli, N. M., & Bagheri, S. (2015). Graphene supported heterogeneous catalysts: An overview. *International Journal of Hydrogen Energy, 40*(2), 948-979.

[19] Morales-Torres, S., Pastrana-Martínez, L. M., Figueiredo, J. L., Faria, J. L., & Silva, A. M. (2012). Design of graphene-based TiO_2 photocatalysts—a review. *Environmental Science and Pollution Research, 19*, 3676-3687.

[20] Li, G., Li, K., Liu, A., Yang, P., Du, Y., & Zhu, M. (2017). 3D flower-like β-MnO_2/reduced graphene oxide nanocomposites for catalytic ozonation of dichloroacetic acid. *Scientific Reports, 7*(1), 43643

[21] Yang, H., Kershaw, S. V., Wang, Y., Gong, X., Kalytchuk, S., Rogach, A. L., & Teoh, W. Y. (2013). Shuttling photoelectrochemical electron transport in tricomponent $CdS/rGO/TiO_2$ nanocomposites.

Journal of Physical Chemistry C, 117(40), 20406-20414.

[22] Loh, K. P., Bao, Q., Ang, P. K., & Yang, J. (2010). The chemistry of graphene. *Journal of Materials Chemistry, 20*(12), 2277-2289.

[23] Puangpetch, T., Sommakettarin, P., Chavadej, S., & Sreethawong, T. (2010). Hydrogen production from water splitting over Eosin Y-sensitized mesoporous-assembled perovskite titanate nanocrystal photocatalysts under visible light irradiation. *International Journal of Hydrogen Energy, 35*(22), 12428-12442.

[24] Wan, D., Wu, L., Liu, Y., Chen, J., Zhao, H., & Xiao, S. (2019). Enhanced adsorption of aqueous tetracycline hydrochloride on renewable porous clay-carbon adsorbent derived from spent bleaching earth via pyrolysis. *Langmuir, 35*(11), 3925-3936.

[25] Merroun, Y., Chehab, S., El Hallaoui, A., Guedira, T., Boukhris, S., Ghailane, R., & Souizi, A. (2023). Triple superphosphate modified by tin (II) chloride: As a reusable and efficient catalyst for the one-pot synthesis of xanthene and xanthenone derivatives under green conditions. *Journal of Molecular Structure*, *1294*, 136383.

[26] Galehban, M. H., Zeynizadeh, B., & Mousavi, H. (2022). Ni II NPs entrapped within a matrix of l-glutamic acid cross-linked chitosan supported on magnetic carboxylic acid-functionalized multi-walled carbon nanotube: a new and efficient multi-task catalytic system for the green one-pot synthesis of diverse heterocyclic frameworks. *RSC advances*, *12*(26), 16454-16478.

[27] Safaei Ghomi, J., Zahedi, S., & Ghasemzadeh, M. A. (2014). AgI nanoparticles as a remarkable catalyst in the synthesis of (amidoalkyl) naphthol and oxazine derivatives: an eco-friendly approach. *Monatshefte für Chemie-Chemical Monthly*, *145*, 1191-1199.

[28] Safaei-Ghomi, J., & Ghasemzadeh, M. A. (2017). Zinc oxide nanoparticle promoted highly efficient one pot three-component synthesis of 2, 3-disubstituted benzofurans. *Arabian Journal of Chemistry*, *10*, S1774-S1780.

[29] Safaei-Ghomi, J., Ghasemzadeh, M. A., & Kakavand-Qalenoei, A. (2016). CuI-nanoparticles-catalyzed one-pot synthesis of benzo [b] furans via three-component coupling of aldehydes, amines and alkyne. *Journal of Saudi Chemical Society*, *20*(5), 502-509

[30] Farhadi, S., Ghasemzadeh, M. A., & Aghaei, S. S. (2019). NiCo2O4@ Ni (BDC) Nano-Porous Metal–Organic Framework as a Novel Catalyst for the Synthesis of Spiro [indene [1, 2-d] pyrimidine-ones and Investigation of Their Antimicrobial Activities. *ChemistrySelect*, *4*(2), 729-736.

[31] Nile, S. H., & Park, S. W. (2015). Chromatographic analysis, antioxidant, anti-inflammatory, and xanthine oxidase inhibitory activities of ginger extracts and its reference compounds. *Industrial Crops and Products*, *70*, 238-244.

[32] Figueiredo, J., Serrano, J. L., Cavalheiro, E., Keurulainen, L., Yli-Kauhaluoma, J., Moreira, V. M., ... & Almeida, P. (2018). Trisubstituted barbiturates and thiobarbiturates: Synthesis and biological evaluation as xanthine oxidase inhibitors, antioxidants, antibacterial and anti-proliferative agents. *European journal of medicinal chemistry*, *143*, 829-842.

[33] Abdulhafiz, F., Mohammed, A., Kayat, F., Bhaskar, M., Hamzah, Z., Podapati, S. K., & Reddy, L. V. (2020). Xanthine oxidase inhibitory activity, chemical composition, antioxidant properties and GC-MS Analysis of Keladi Candik (Alocasia longiloba Miq). *Molecules*, *25*(11), 2658.

[34] Samiee Paghaleh, E., Dashtian, K., Yousefi Seyf, J., Seidi, F., & Kolvari, E. (2023). Green Synthesis of Stable CuFe$_2$O$_4$/CuO-rGO Heterostructure Photocatalyst Using Basil Seeds as Chemo-reactors for Improved Oxytetracycline Degradation. *Journal of Environmental Chemical Engineering*, 110676.

[35] Phuruangrat, A., Kuntalue, B., Thongtem, S., & Thongtem, T. (2016). Synthesis of cubic CuFe$_2$O$_4$ nanoparticles by microwave-hydrothermal method and their magnetic properties. *Materials Letters, 167*, 65-68.

[36] Anselmi, C., Capitani, D., Tintaru, A., Doherty, B., Sgamellotti, A., & Miliani, C. (2017). Beyond the color: a structural insight to eosin-based lakes. *Dyes and Pigments, 140*, 297-311.

[37] Ahmad, M. A., Eusoff, M. A., Oladoye, P. O., Adegoke, K. A., & Bello, O. S. (2020). Statistical optimization of Remazol Brilliant Blue R dye adsorption onto activated carbon prepared from pomegranate fruit peel. *Chemical Data* Collections*, 28*, 100426.

[38] Huang, X.-Y., Bin, J.-P., Bu, H.-T., Jiang, G.-B., & Zeng, M.-H. (2011). Removal of

anionic dye eosinY from aqueous solution using ethylenediamine modified chitosan. *Carbohydrate Polymers, 84*(4), 1350-1356.

[39] Peluso, P., Mamane, V., Dessì, A., Dallocchio, R., Aubert, E., Gatti, C., Cossu, S. (2020). Halogen bond in separation science: A critical analysis across experimental and theoretical results. *Journal of Chromatography A, 1616*, 460788.

[40] Wang, H. K., Morris-Natschke, S. L., & Lee, K. H. (1997). Recent advances in the discovery and development of topoisomerase inhibitors as antitumor agents. *Medicinal* Research *Reviews, 17*(4), 367-425.

[41] Mardare, D. (2000). MT asca, M. Delibas and GI Rusu. *Applied Surface Science, 156*, 200.

[42] Yahia, I., & Keshk, S. M. (2017). Preparation and characterization of PVA/Congo red polymeric composite films for a wide scale laser filters. *Optics & Laser Technology, 90*, 197-200.

[43] Liu, X., Cong, T., Liu, P., & Sun, P. (2016). Synthesis of 1, 2-diketones via a metal-free, visible-light-induced aerobic photooxidation of alkynes. *Journal of Organic Chemistry, 81*(16), 7256-7261.

[44] Singh, M., Yadav, A. K., Yadav, L. D. S., & Singh, R. (2018). Synthesis of 6-thiocyanatophenanthridines by visible-light- and air-promoted radical thiocyanation of 2-isocyanobiphenyls. *Synlett, 29*(02), 176-180.

[45] Rabiei, kh., & Mostafapour, Z . (2022). Functionalized nanoclinoptilolite: a new and suitable nanocatalyst for the synthesis of xanthene dione green derivatives in solvent-

free conditions. *Applied Chemistry*,17(64),44-27. (in persion)

[46] M Hosseini, M., Kolvari, E., Vahidian, M., & Bagheri, R. (2016). Nano perlite sulfuric acid: an inexpensive heterogeneous acid catalyst for the synthesis of 1, 8-dioxo-octahydroxanthenes and tetrahydrobenzoxanthenes under solvent-free conditions. *Applied Chemistry*, 11(41), 109-118 (in persion).

[47] Kazemi Rad, R., & Azizian, J. (2015). One-pot synthesis of 2, 2'-Arylmethylene bis (3-hydroxy-5, 5-dimethyl-2-cyclohexene-1-one) by electrochemical method. *Applied Chemistry*, 10(36), 45-52. (in persion)

[48] Tabrizian, E., & Amuzadeh, A. *(*2014). Synthesis of xanthene derivatives based on α,/α-bis(benzylidene)cycloalkanones using tungsten phosphoric acid catalyst under solvent-free conditions. *Applied Chemistry*, 9(30), 23-30. (in persion)

[49] Nikpasand, M., Zare Fekri, L. (2019). Synthesis of novel multicomponent 9-aryl-2H-xanthene-8,1(2H)-diones with diazo bridge using ionic liquid [BDBDMIm]HSO_4. *Applied Chemistry*, 14(51), 325-336. (in persion)

[50] Yıldız, Y., Esirden, İ., Erken, E., Demir, E., Kaya, M., & Şen, F. (2016). Microwave (Mw)-assisted Synthesis of 5-Substituted 1H-Tetrazoles via [3+ 2] Cycloaddition Catalyzed by Mw-Pd/Co Nanoparticles Decorated on Multi-Walled Carbon Nanotubes. *ChemistrySelect, 1*(8), 1695-1701.

[51] Song, G., Wang, B., Luo, H., & Yang, L. (2007). Fe^{3+}-montmorillonite as a cost-effective and recyclable solid acidic catalyst

for the synthesis of xanthenediones. *Catalysis Communications, 8*(4), 673-676.

[52] Maghsoodlou, M. T., Habibi-Khorassani, S. M., Shahkarami, Z., Maleki, N., & Rostamizadeh, M. (2010). An efficient synthesis of 2, 2′-arylmethylene bis (3-hydroxy-5, 5-dimethyl-2-cyclohexene-1-one) and 1, 8-dioxooctahydroxanthenes using ZnO and ZnO–acetyl chloride. *Chinese Chemical Letters, 21*(6), 686-689.

[53] Kahandal, S. S., Burange, A. S., Kale, S. R., Prinsen, P., Luque, R., & Jayaram, R. V.

(2017). An efficient route to 1,8-dioxo-octahydroxanthenes and-decahydroacridines using a sulfated zirconia catalyst. *Catalysis Communications, 97*, 138-145.